Weld World (2018) 62:1–8
DOI 10.1007/s40194-017-0515-0

RESEARCH PAPER

Evaluation of microstructure and mechanical properties of P91 steel weldment due to addition of boron trioxide into flux during submerged arc welding

Joydeep Roy[1] · **Ram Naresh Rai**[2] · **Subhash Chandra Saha**[1]

Received: 3 February 2017 / Accepted: 20 September 2017 / Published online: 5 October 2017

Abstract The present investigation studied the effect of boron trioxide (B_2O_3) addition into flux on the microstructure and mechanical properties of modified 9Cr-1Mo (P91) steel in submerged arc welding (SAW) process. Boron trioxide powder was mixed with commercial flux in different ratios to change the weld metal chemical composition. Optical emission spectroscopy results showed that weight percentage of boron varies from 0.00 to 0.0068 with the addition of boron trioxide into welding flux. Weld metal microstructure without the addition of boron reveals the presence of tempered martensite and ferrite phase, whereas boron-added microstructures highlighted the dominating nature of tempered martensite. Scanning electron microscope analysis also showed that the dispersed carbides especially $M_{23}C_6$ were increased with the addition of boron. Weld metal macrohardness profile reveals that boron has the significant effect on the weld metals. The maximum hardness of 342 HV was found for the 12.5% B_2O_3, whereas weld of without boron shows the hardness of 240.8 HV. Boron addition has a positive effect on the tensile strength of weld joints except for the 12.5% B_2O_3. But the toughness of weld zone decreases with the addition of boron.

Keywords (IIW Thesaurus) P91 steel · Boron · Microstructure · Mechanical properties · Saw

Recommended for publication by Commission II - Arc Welding and Filler Metals

✉ Joydeep Roy
deeproymech@gmail.com

Ram Naresh Rai
nareshray@yahoo.co.in

Subhash Chandra Saha
subashchandrasaha@yahoo.in

[1] Department of Mechanical Engineering, National Institute Technology Agartala, Jirania, India

[2] Department of Production Engineering, National Institute Technology Agartala, Jirania, India

1 Introduction

The biggest threat to the civilization of twenty-first century is the global warming. Reduction of CO_2 emission is an urgent task for power industries, especially for fossil power plants. Their thermodynamic efficiency can be increased by increasing the steam entering temperature and pressure to the turbines [1, 2]. Therefore, materials having high creep strength, high thermal conductivity, and low expansion coefficient must be selected for high-temperature components to withstand such strenuous conditions. It has been seen that body-centered cubic (BCC) iron has the great advantage over the austenitic steels due to its low thermal expansion coefficient and high thermal conductivity [3]. These properties permit ferritic alloys to resist thermal fatigue when implemented in thick sections for the construction of power plant, even though the austenitic variants may be stronger in creep. Nine to twelve percent Cr martensitic/ferritic steels show significant high-temperature materials for fossil-fired plants operating at a temperature up to 600 °C [4]. These steels are widely used as structural materials in power plants such as steam headers, steam lines, pipes, or high-temperature boilers and turbine parts. Cr-Mo steel alloys have shown susceptibility to a number of phenomena, particularly in the case of welds, which invariably have the potential to reduce efficiency and shorten service life [5]. The problems encountered in welding joints of these steels under creep conditions, both in base metal (BM) and weld metal (WM), are the result of type-IV cracking, i.e.,

crack initiation in the region of the heat-affected zone (HAZ), immediately next to the BM [6].

In order to achieve excellent high-temperature strength, many kinds of strengthening elements have been added to the conventional Cr-Mo steels. Chromium is a solid-solution strengthener and carbide former, which makes Cr as the main alloying element of P91 steel as well as heat-resistant ferritic/martensitic steels [7]. The strengthening effect is achieved by the precipitation of chromium-rich carbides from the solid solution, which can impede the movement of dislocations and grain boundaries to increase creep strength of the steels. The chromium carbides M_7C_3 and $M_{23}C_6$ are two main chromium carbide types in chromium steels; $M_{23}C_6$ dominates in the 9–12% Cr steels [8]. Molybdenum is the second most important element of P91 steel which is also a ferrite stabilizer. It improves the creep properties of the steels by solid-solution hardening [9]. However, molybdenum can be detrimental because it accelerates the growth of $M_{23}C_6$ carbides [10]. Molybdenum can form Mo_2C in low-chromium steels, such as 2.5Cr-1Mo steel, but it does not from carbides or nitrides in 9–12% Cr steels [11]. It has been found that boron can segregate to the interface between $M_{23}C_6$ particles and the matrix to decrease the rate at which the carbide can coarsen, thus stabilizing the microstructure, since $M_{23}C_6$ particles help in pinning the subgrain boundaries [12]. It is also found that boron assists in the nucleation of VN particles by the mechanism of latent creep resistance [13]. They can combine with vacancies to reduce the self-diffusion coefficient of ferrite matrix. They can also form a cottrell atmosphere around dislocations and thus increase creep deformation resistance [14].

The above study reveals that the role of boron for the Cr-Mo is very vital as far as high-temperature application is concerned. So the aim of the present investigation is to study the influence of boron trioxide additions in the fluxes on the microstructure and mechanical properties of the P91 submerged arc welded plates.

2 Experimental details

2.1 Materials

Modified 9Cr-1Mo (P91) steel plate which is more suitable for fabrication of heavy-duty products under high-temperature operating condition was considered as base metal in this present investigation. The trade name of the base metal SA387 grade 91 class 2 and the thickness is 10 mm. The base metal was normalized at 1050 °C for 0.5 h followed by air cooling and tempered at 770 °C for 2 h with subsequent air cooling during its fabrication stage, and the entire plate was ultrasonically tested by the supplier. The chemical composition of base metal was analyzed by using optical emission spectroscopy (OES) as given in Table 1.

The dimension of base metal was taken as 200 × 100 × 10 mm^3. The selection of appropriate SAW wire and flux is a very important stage for SAW process to obtain good weld joint with significant properties. The composition of wire and flux should be such that it should match the overall chemistry of the weld joint. Consumables for P91 steel were supplied by D&H Scheron electrodes pvt. ltd. Electrode wire grade is AWS.SFA.5.23 EB9 having diameter of 3.15 mm, and the flux used for welding was MAX flux SAF12.

2.2 Experimental procedure

The goal of the present work is to see the effect of boron trioxide addition into flux on the microstructure and mechanical properties in submerged arc weld metals. For that purpose, the welding process parameters were kept constant and welding was performed on square butt joint. Welding process parameters are given in Table 2.

Boron trioxide powder was mixed in different ratios with commercial flux for making the various weld metals composition. These powders were mixed in a small rotating drum with the fresh commercial flux in amounts of 2.5, 5.0, 7.5, 10.0, and 12.5%. Beyond this maximum limit, powder could not be added because after that limit, welding is not good (visual inspection) and detachability of slag is also poor. A fresh flux (without any addition of B_2O_3) welding was made for the comparison. The pre-heat temperature of 200–250 °C was maintained throughout the welding. A post weld heat treatment (PWHT) was performed at 760 °C for 3 h then cooled to room temperature in the furnace.

Samples were polished using different grades of emory papers up to 2000 grit in an automatic polishing machine; then, fine finishing was performed using 1 and 0.5 μm diamond paste on a selvyt cloth. Samples of P91 steel were etched by viella's solution (2 g picric acid, 5 ml HCl, 90 ml ethyl alcohol). Evaluation of chemical composition of WM is the important step in this present investigation to quantify the weight percentage of boron in the WM. Optical emission spectroscope processed from M/s Jobinyvon, France model no. 132F was used for analysis of chemical composition of base metal as well as weld metals. Specimens of 25 mm × 25 mm × 10 mm were mechanically grounded up to 400 grit paper and used for analysis. An optical microscope (LEICA DMI 3000M) attached with an image-analyzing software was used in this present investigation. Grain size measurement was performed by following linear intercept method as per ASTM E112 in the image analyzing software with 95% confidence level [15]. A ZEISS EVO 60 SEM (MODEL-8113) equipped with light element INCA energy dispersive X-ray spectroscopy (EDX) was also used to acquire micrographs of the weld metals and inclusions at high magnification. Hardness testing was carried in a macrohardness testing machine model—Matsuzawa MMT-X7B. Vickers hardness testing was carried out in a straight line

Table 1 Base metal chemical composition (wt%)

Element	C	Mn	P	S	Cr	Ni	Mo	Nb	Al	V	N
P91	0.105	0.432	0.014	0.0008	8.975	0.228	0.855	0.075	0.013	0.202	0.006

2 mm below and parallel to the surface of the base metal with a constant load of 1 kg and dwell time 10 s by following ASTM E384-11e [16]. Tensile testing was performed in compliance with ASTM E8M [17]. Tensile samples were prepared in round type, small size proportional to standard having the gauge length 30 mm, fillet radius 6 mm, diameter 6 mm, and length of reduced section 36 mm. The off-set method was used to find out the yield strength, and the other readings were found from the software. The strain rate was 0.5 mm/min and experiments were performed at room temperature. For impact testing, charpy V-notch impact toughness samples were prepared according to the ASTM E23 standard [18]. The dimension of the sample was 75 mm × 10 mm × 10 mm, i.e., standard size. Machining was done in wire electric discharge machine and the nose radius was equal to 0.25 mm, nose angle 45°, notch depth 2 mm, and anvil radius 0.66 mm; test temperature was at room temperature.

3 Results and discussion

3.1 Changes in weld metal chemical composition

The weld metal chemical composition analysis was conducted by optical emission spectroscopy, and the results are provided in Table 3. The weld metal chemical composition results show that the values for each element are fairly uniform, except the boron, which varied systematically from 0.00 to 0.0068%.

3.2 Microstructure evaluation

P91 base metal consists of fully tempered martensite matrix, with finely dispersed carbides, and carbo-nitrides precipitation on the grain boundaries. The carbides are of $M_{23}C_6$ type, M being metallic elements, mainly Cr and Fe, Mn, and Mo if present; and the grain boundary carbonitrides are of MX type, M being Nb and V, and X being C and N [19].

Table 2 Welding process parameters

Parameters	Units	
Wire feed rate	mm/min	200
Stickout	mm	28
Traverse speed	m/min	0.45
Voltage	Volt	34
Current	A	625

In the as-welded condition, P91 electrodes produce a predominantly untempered martensitic structure in which the solidification substructures are not seen. Microstructural evidence for martensitic transformation for PWHT above the AC1 temperature was available after etching the specimens with the LePera regent, which reveals the fresh martensite and ferrite in white and tempered martensite and bainite in a dark color [20]. Figures 1 and 2 show the microconstituent percentage, as well as the mean width of different phases, was determined by means of quantitative metallography. Phase analysis of weld metal depicts that addition of B_2O_3 has the significant effect on the phases. Ferrite percentage decreases with the addition of boron. The minimum grain size is found for the P91B5 condition.

SEM micrographs show finely dispersed precipitates in all weld metals. Precipitates are mainly aligned along the prior austenite grain and the martensitic lath boundaries. Some finer precipitates can be observed inside the martensitic laths. SEM micrographs with different percentages of B_2O_3 addition reveal the changes in precipitation quantity and formation of carbides as shown in Fig. 3, respectively. It has been seen that with the addition of boron, precipitation percentage has been increased. Weld metal SEM micrograph reveals the typical tempered martensite and ferrite microstructure of P91 steel weld metal. Phase analysis in optical microscope by using Image analyzing software depicts that martensite percentage increases with addition of boron content in the weld metal. Diffraction pattern as shown in Fig. 4 provides the evidence of martensite formation in the weld metal during tempering.

Micrographs reveal that carbide ($M_{23}C_6$) precipitate percentage increases with the increase of boron content. The $M_{23}C_6$ carbides are distributed mainly along prior austenite grain boundaries and along martensite lath, block, and packet boundaries inside the grain [21]. $M_{23}C_6$ is the main precipitates in most heat-resistant steels. Generally, this carbide is chromium rich, with Fe, Ni, Mn, and Mo substitute for Cr partially, and the fraction of these substitute atoms can be up to 40% [22]. The crystal structure of $M_{23}C_6$ is a complex face-centered cubic (fcc) with a parameter about 1.06 nm, which changes slightly for metallic element variation [23]. $M_{23}C_6$ is a very stable precipitation in structure, but they coarsen obviously during creep exposure at elevated temperature. Boron can only improve the creep behavior if it is either enriched in other precipitates or dissolved in the matrix [24].

EDX analysis of precipitates has shown that they were rich in iron and chromium. All these precipitates are apparently formed during auto-tempering as discussed earlier [1]. From the EDX analysis of inclusions, it was observed that

Table 3 Weld metal chemical composition with various B_2O_3 (wt%)

Element	C	Mn	Si	P	S	Cr	B	V	Mo	Nb	Al	N
P91B0	0.096	0.55	0.36	0.014	0.0071	9.82	0.0000	0.201	0.96	0.077	0.018	0.0056
P91B2.5	0.092	0.52	0.349	0.013	0.0072	9.59	0.0018	0.196	0.97	0.074	0.016	0.0059
P91B5	0.092	0.53	0.323	0.016	0.0077	9.92	0.0024	0.198	0.96	0.077	0.014	0.0057
P91B7.5	0.093	0.57	0.34	0.012	0.007	9.7	0.0036	0.195	0.95	0.076	0.012	0.0055
P91B10	0.09	0.52	0.323	0.015	0.0076	9.92	0.0049	0.201	0.96	0.078	0.016	0.0057
P91B12.5	0.098	0.498	0.332	0.016	0.0068	9.62	0.0068	0.20	0.99	0.079	0.018	0.0058

increasing the boron trioxide content leads to a change in the oxide proportion of the material. With increasing boron trioxide content in the weld, the oxide content in the inclusions increases gradually and it varies with different B_2O_3 as 11.26, 16.42, 20.75, 23.83, 29.46, and 35.61%, respectively.

3.3 HAZ

Figure 5 shows the optical micrographs of coarse grain HAZ (CGHAZ) and fine grain HAZ (FGHAZ) of boron containing P91 steel. The stronger influence of peak temperature over pinning effect produces relatively coarser grains than the unaffected base metal; this region is known as CGHAZ, where peak temperature experienced is just above the AC_1 temperature; chromium-rich carbides do not dissolve completely [12]. The presence of this type of precipitate as well as MX type of precipitates in this region. The average grain size of black and white phase in the CGHAZ is 11.5 and 10.9 μm. Fine-grained austenite is produced, which subsequently transforms into low-carbon slit softer martensite as shown in Fig. 5. The austenitized FGHAZ transforms to martensite on cooling. The average grain size of black and white phase in the FGHAZ is 10.5 and 10.1 μm. The new austenite nucleates at the prior austenite grain boundaries and the martensite lath boundaries, whereas the remainder of the microstructure is simply tempered [17]. The austenite transforms into untempered martensite on cooling. The average grain size of black and white phase in the intercritical (ICHAZ) is 9.3 and 9.2 μm.

3.4 Hardness profile with various B_2O_3%

A macrohardness profile across both columnar and refined regions on a transverse section of P91 weld metal in the as-PWHT condition is shown in Fig. 6. In the as-welded condition, the P91 steel welds exhibit a hardness of about 400 HV because of their untempered martensitic structure. It can be seen that columnar region exhibits a much higher hardness than the refined region. The hardness profile shows that boron has a significant effect on the WM hardness, which shows the hardenability effect of boron. Maximum hardness has been found in the highest B_2O_3 percentage. Hardness of HAZ does not show any appreciable improvement with boron content. The hardness values in the columnar regions range from 258 to 342 HV with the B_2O_3 percentage, whilst the hardness values in the refined regions decrease gradually and became steady at the base metal. In the CGHAZ, the hardness value varies from 250 to 340 HV. After that, in FGHAZ, hardness is

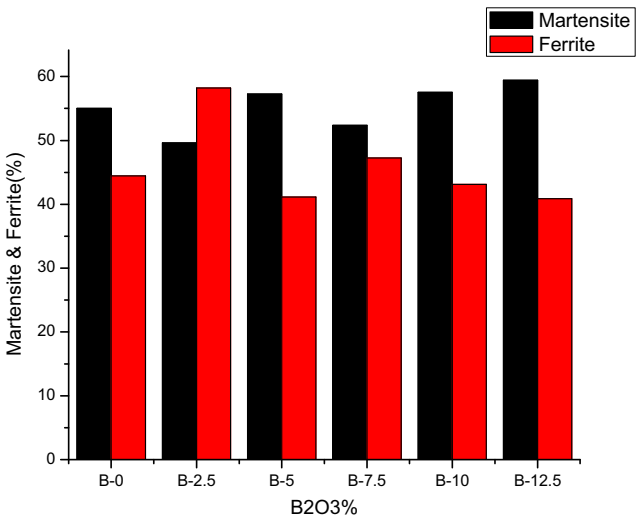

Fig. 1 Phase analysis of P91 WM with boron

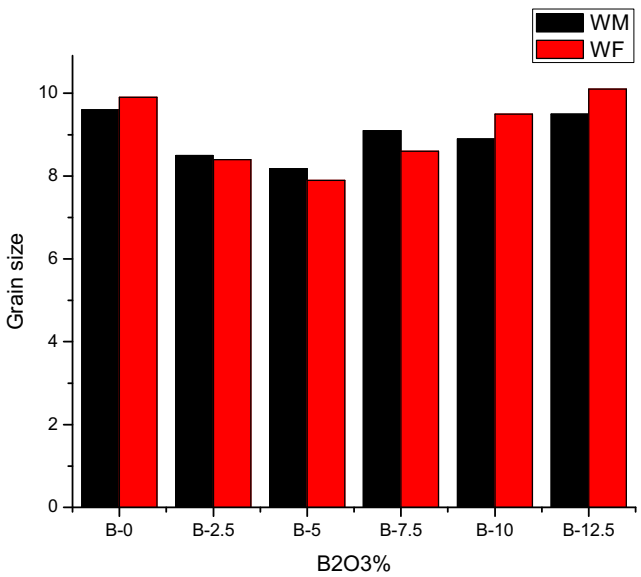

Fig. 2 Effect of boron on the grain size of WM

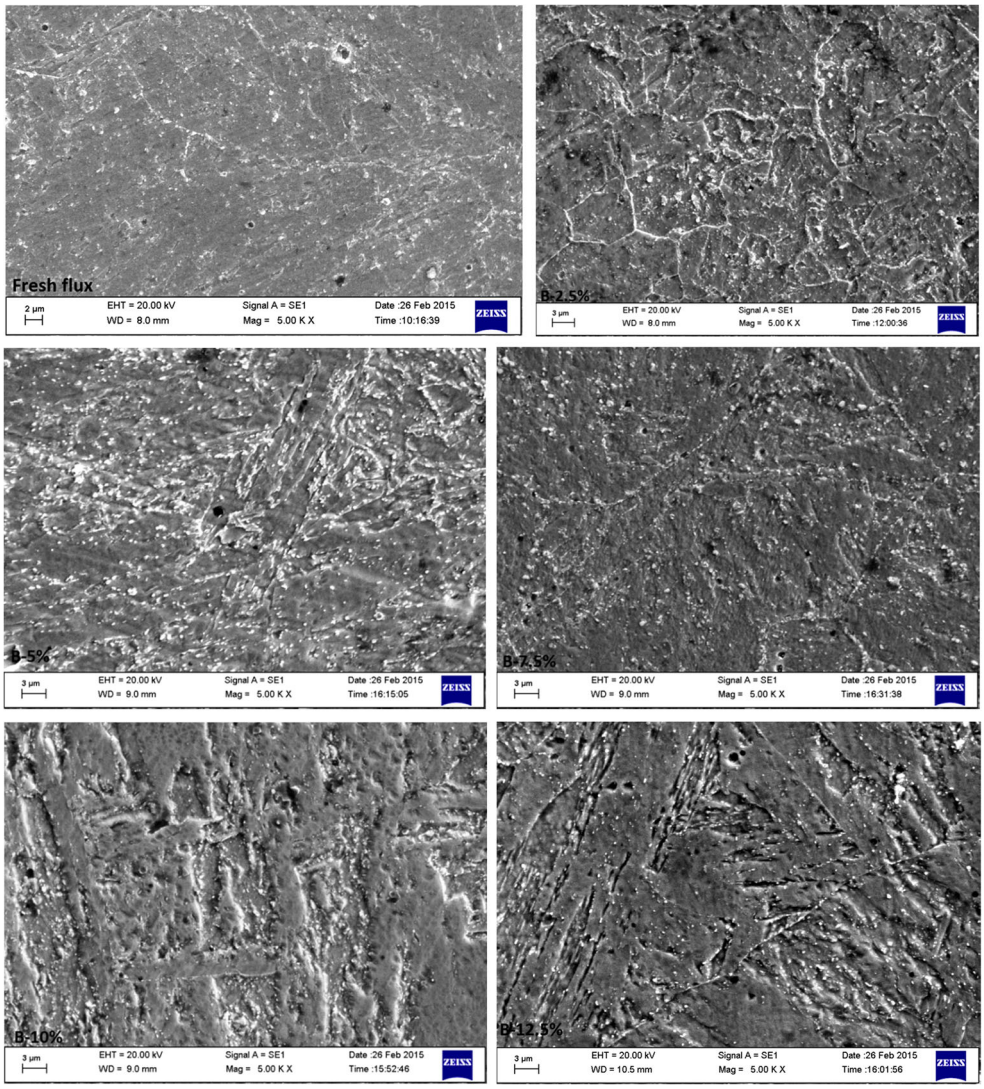

Fig. 3 SEM micrographs of B_2O_3-added weld metal

decreasing drastically and varies in between 190 and 250 HV with respect to B_2O_3addition. ICHAZ is showing the minimum hardness in HAZ, where the hardness varies within 190–200 HV. Improvement of hardness has a positive effect on the creep strength which is the main objective of this material. The base metal is showing the hardness of 170–180 HV after tempering. Ohtsuka et al. [25] reveal an interesting correlation between creep rupture strength and the hardness of normalized-and-tempered P91 steel. They have found that the creep strength linearly increases with increasing of hardness up to 385 HV in the P91 steels. Both creep strength and Vickers hardness of the P91 would be closely correlated with the number density of oxide particles. This correlation may lead to the linear relationship between Vickers hardness and creep strength.

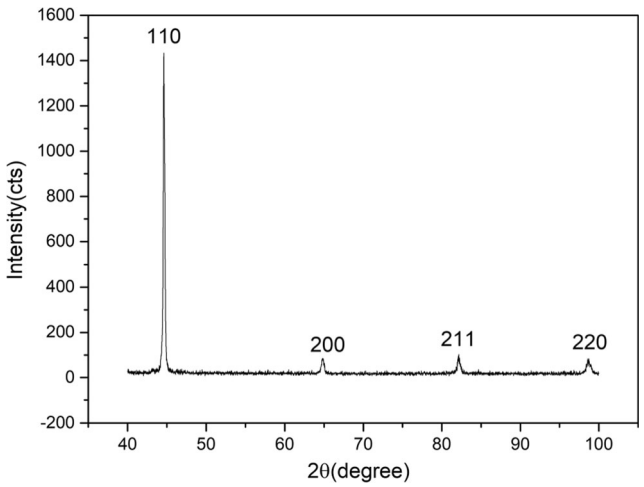

Fig. 4 Diffraction plot of the weld metal for P91B5

3.5 Tensile strength

Figure 7 shows the yield strength (YS) and ultimate tensile strength (UTS) values with different B_2O_3 percentage. Two transverse tensile tests were performed on all welds in accordance with ASTM standard E8M. It is clear from the figure that

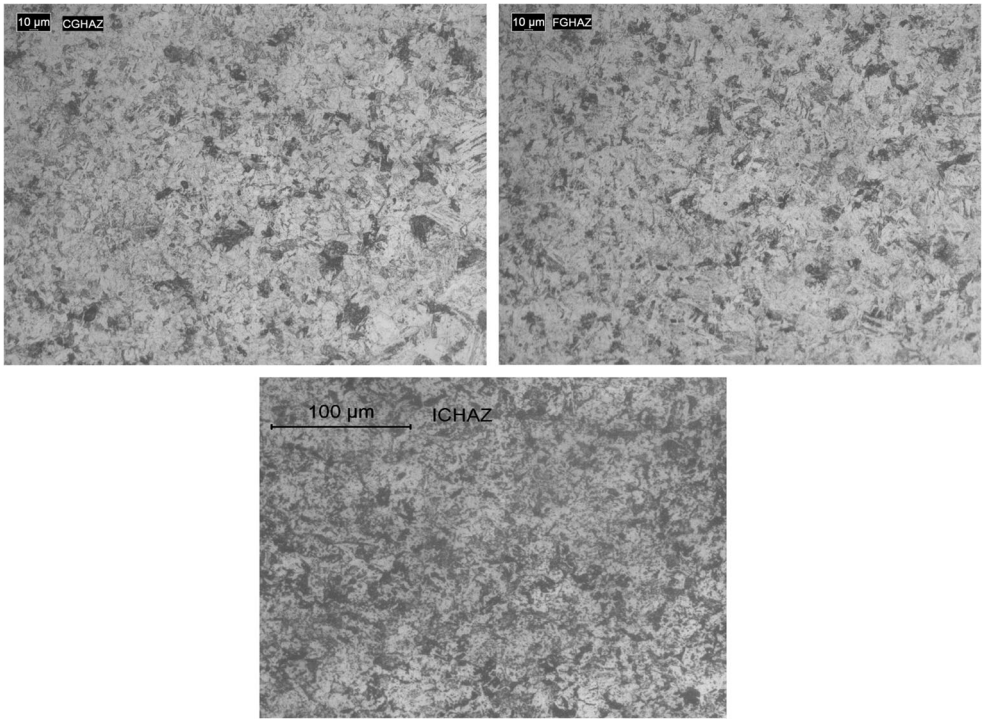

Fig. 5 Optical micrographs of HAZs

the addition of B_2O_3 has a significant effect on YS and UTS. The tensile strength of boron-enriched P91 weld metals is appreciably greater than the without boron WM. The tensile strength value improves with the addition of B_2O_3 up to P91B10 but for the highest B_2O_3 percentage, tensile strength falls. This may be due to the high oxide percentage, which produces macro inclusion. Boron-added WM produces higher tensile strength than the base metal. This could be due to slower recovery and coarsening of lath and precipitates in the presence of boron. Kimmins and Gooch [26] reported that the presence of boron in martensitic steel reduced recovery during tempering. So, the effect of tempering and high-temperature tensile test establishes that the presence of boron imparts stability to the microstructure. The fracture was taken place in the HAZ (in between FGHAZ and CGHAZ) for all tensile specimens. This means that the ICHAZ is the most crucial for P91 weld joint.

The literature suggests that in the presence of boron, interfacial energy decreases which delays initiation of the formation of

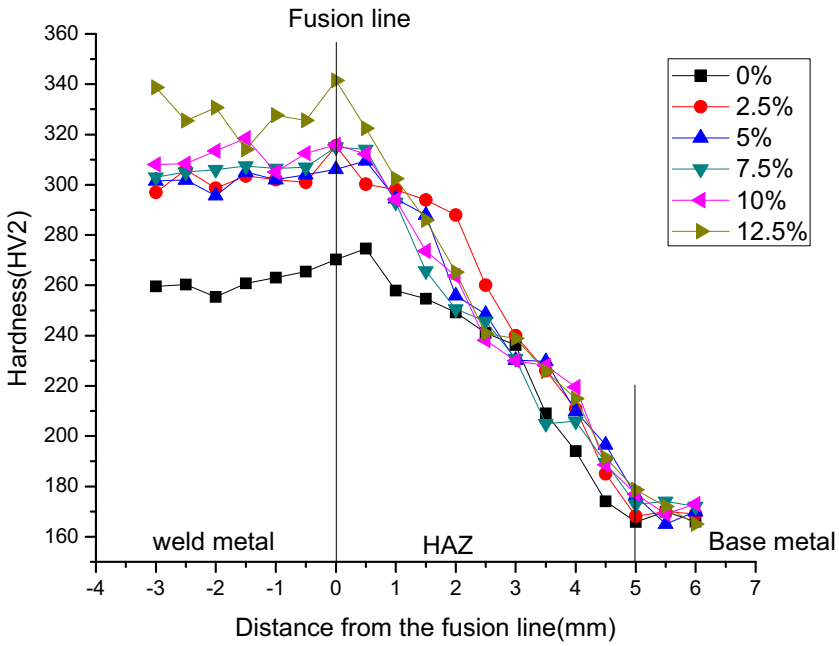

Fig. 6 Hardness profile of weldment in different B_2O_3%

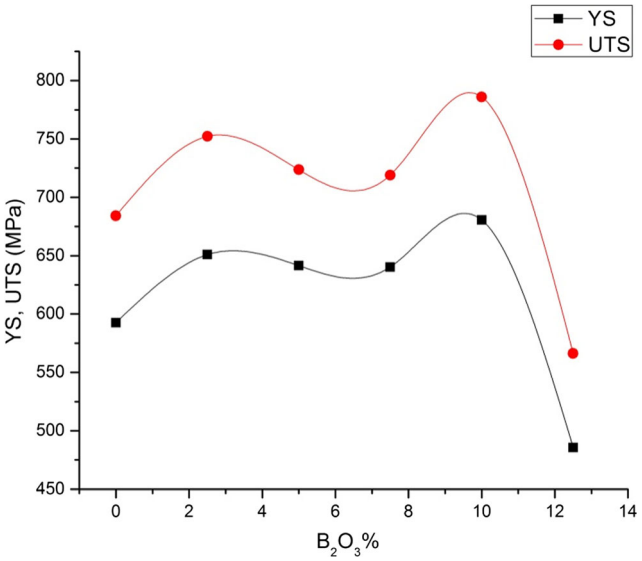

Fig. 7 Effect of B_2O_3 on ultimate of tensile strength

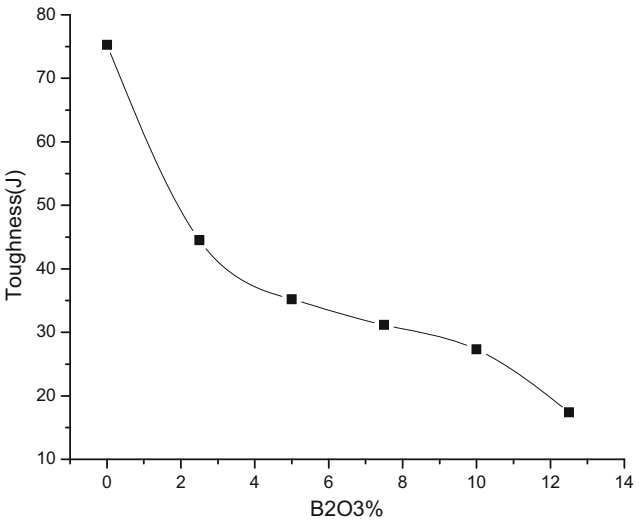

Fig. 9 Effect of B_2O_3 on toughness of the weld zone

cavities and growth due to these precipitates during tensile tests. During tensile test, cavities nucleate at the inclusions or second-phase matrix interface when the material reaches ultimate tensile strength [25, 26]. But for the maximum percentage of boron addition, the tensile strength value falls abruptly; this may be due to the high oxide content exist in the weld metal.

Secondary electron images illustrate the fracture morphology of the weld metal of P91B5 as shown in Fig. 8. The fracture surface of the weld metal is mostly dimple features, which shows the characteristics of the ductile fracture. The fine microstructure explains the improvement in mechanical properties of the weldment.

3.6 Toughness

The results of Charpy impact testing of welds at room temperature exhibit a poor toughness of less than 20 J in the as-welded condition. The absorbed energy increases with the duration of PWHT, and this effect becomes progressively greater as tempering time and temperature are increased [27]. Figure 9 shows the trend of toughness curve with B_2O_3 addition, which reveals the negative effect of B_2O_3 onto the toughness of weld metal. The toughness value gradually decreases with the increase of boron content. This may be due to the effect of carbide presence, which increases with the addition of higher percentages of B_2O_3. Packets and blocks are the basic microstructural units controlling the strength and fracture toughness of the martensitic steels because their boundaries act as barriers for deformation and fracture [12].

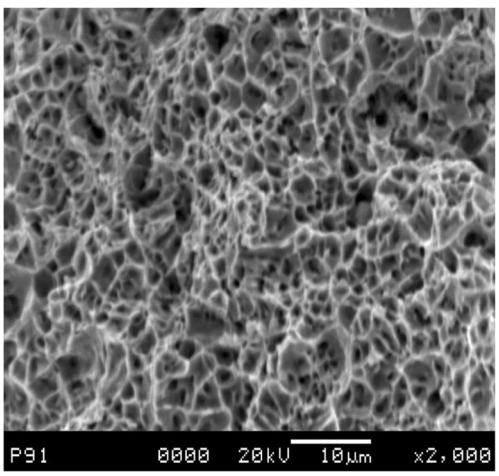

Fig. 8 Fracture surface on tensile specimen

4 Conclusion

P91 base metal consists of mainly tempered martensite matrix, with finely dispersed carbides, and carbo-nitrides precipitation on the grain boundaries. Addition of boron trioxide into the flux is a useful method to change the weld metal chemical composition. Weld metal chemical composition shows that boron varies in the range of 0.00–0.0068 wt%. SEM micrograph shows the precipitation occurs in prior austenite grain boundaries. With the addition of boron precipitation percentage in the grain boundaries increases. Phase analysis of weld metal shows that the volume fraction of martensite increases with the boron content.

The Hardness of weld metal is above 400 HV in as-welded condition which validates the presence of untempered martensite. After tempering, hardness varies in between HV 280–320. B has a significant effect on the hardness. Hardness value of weld metal increases gradually with the addition of boron trioxide. The development of occurs mainly due to the formation of carbides and nitrides into the grains. This could be beneficial for the high-temperature application as far as the literatures are concerned. Hardness value of

boron-added weld metal was found higher compare to that of without boron-added weld metal. Toughness value is not showing any appreciable improvement with the addition of boron. Tensile strength value significantly improves with the addition of boron. At maximum percentage of boron YS and UTS decreased, this may be due to the excess of oxide content into the weld metal.

Compliance with ethical standards

Conflict of interest The authors declare that they have no conflict of interest.

References

1. Agyakwa P (2004) Creep and microstructural development in P91 weldments at elevated temperature. PhD diss., University of Nottingham
2. Vaillant, J. C., B. Vandenberghe, B. Hahn, H. Heuser, and C. Jochum. T/P23, 24, 911 and 92: new grades for advanced coal-fired power plants—properties and experience. Int J Press Vessel Pip 85, 1 38–46, 2008
3. Haarmann K, Vaillant JC, Bendick W, Arbab A (1999) The T91/P91 Book. Vallourec & Mannesmann Tubes
4. Zhang Y (2009) Changes in microstructure and mechanical properties of P91 weld metal during creep. PhD diss., University of Nottingham
5. Kamal HD, Vishvesh JB (2015) Effect of activating fluxes on weld bead morphology of P91 steel bead-on-plate welds by flux assisted tungsten inert gas welding process. J Manuf Process 17:48–57
6. Das CR (2011) Influence of boron on microstrcture and mechanical properties of modified 9cr-1mo steel weldments Ph. D thesis, 2011, IIT Madras
7. Klueh RL (2005) Elevated temperature ferritic and martensitic steels and their application to future nuclear reactors. Int Mater Rev 50:287–310
8. Sourmail T (2001) Precipitation in creep resistant austenitic stainless steels. Mater Sci Technol 17(1):1–14
9. Maruyama K, Sawada K, Koike J-i (2001) Strengthening mechanisms of creep resistant tempered martensitic steel. ISIJ Int (Japan) 41(6):641–653
10. Anderson P, Bellgardt T, Jones FL (2003) Creep deformation in a modified 9Cr-1Mo steel. Mater Sci Technol 19:207–213
11. Nutting, J. (1999) The structural stability of low alloy steels for power generation applicationsLondon, IOM Communications Ltd, 12–30
12. Albert SK, Kondo M, Tabuchi M, Yin F, Sawada K, Abe F (2005) Improving the creep properties of 9Cr-3W-3Co-NbV steels and their weld joints by the addition of boron. Metall Mater Trans A 36(2):333–343
13. Abe F, Horiuchi T, Taneike M, Sawada K (2004) Stabilization of martensitic microstructure in advanced 9Cr steel during creep at high temperature. Mater Sci Eng A 378(1):299–303
14. Horiuchi, T., Masaaki, I., and F. Abe. Improved utilization of added B in 9Cr heat-resistant steels containing W. ISIJ Int 42, no. Suppl P (2002): S67-S71
15. ASTM E-112 (2010) Standard test methods for determining average grain size
16. ASTM E384–11e1 (2011) Standard test method for knoop and vickers hardness of materials
17. ASTM E8M–04 (2008) Standard test methods of tension testing of metallic materials
18. ASTM E23 (2006) Standard methods for notched bar impact testing of metallic materials
19. Silwal B, Li L, Deceuster A, B. Griffiths (2013) Effect of postweld heat treatment on the toughness of heat-affected zone for grade 91 steel. Weld J 92(3)
20. LePera FS (1980) Improved etching technique to emphasize martensite and bainite in high-strength dual-phase steel. J. Met 32(3): 38–39
21. Milović L, Vuherer T, Blačić I, Vrhovac M, Stanković M (2013) Microstructures and mechanical properties of creep resistant steel for application at elevated temperatures. Mater Des 46:660–667
22. Hu Z-F, Yang Z-G et al (2004) An investigation of the embrittlement in X20CrMoV12.1 power plant steel after long-term service exposure at elevated temperature. Mater Sci Eng A 383:224–228
23. Taneike M, Abe F, Sawada K (2003) Creep-strengthening of steel at high temperatures using nano-sized carbonitride dispersions. Nature 424(6946):294–296
24. Hu Z, Yang Z (2003) Identification of the precipitates by TEM and EDS in X20Cr MoV12.1 for long-term service at elevated temperature. J Mater Eng Perform 12(1):106–111
25. Ohtsuka S, Ukai S, Fujiwara M, Kaito T, Narita T (2005) Improvement of creep strength of 9CrODS martensitic steel by controlling excess oxygen and titanium concentrations. Mater Trans 46(3):487–492
26. Kimmins ST, Gooch DJ (1983) Austenite memory effect in 1Cr–1 Mo–0.75V(Ti, B) steel. Mater Sci 17:519–521
27. Yoshino M, Mishima Y, Toda Y, Kushima H, Sawada K, Kumura K (2005) Phase equilibrium between austenite and MX carbonitride in a 9Cr-1Mo-V-Nb steel. ISIJ Int 45:107–115